

## Electronic Supplementary Information (ESI)

### Tailoring the catalytic active sites in Co-based catalysts for electrochemical methanol upgrading to produce formate

Yameng Wang,<sup>†,a</sup> Xue Yang,<sup>†,a</sup> Kexin Wang,<sup>a</sup> Zimeng Liu,<sup>a</sup> Xiaoning Sun,<sup>a</sup> Jinyue Chen,<sup>a</sup> Shanshan Liu,<sup>b</sup> Xu Sun,<sup>c</sup> Junfeng Xie<sup>\*,a</sup>, Bo Tang<sup>\*,a</sup>

*a College of Chemistry, Chemical Engineering and Materials Science, Key Laboratory of Molecular and Nano Probes (Ministry of Education), Collaborative Innovation Center of Functionalized Probes for Chemical Imaging in Universities of Shandong, Institute of Molecular and Nano Science, Shandong Normal University, Jinan, Shandong, 250014, China. E-mail: xiejf@sdsu.edu.cn; tangb@sdsu.edu.cn.*

*b College of Chemical Engineering and Safety, Binzhou University, Binzhou 256603, China*

*c Key Laboratory of Interfacial Reaction & Sensing Analysis in Universities of Shandong, School of Chemistry and Chemical Engineering, University of Jinan, Jinan 250022, Shandong, P. R. China.*

<sup>†</sup> These authors contributed equally to this work.

## **S1. Characterizations and details in electrocatalytic study**

### **S1.1 Structural characterizations**

The X-ray diffraction (XRD) was performed on a Philips X'Pert Pro Super diffractometer with Cu K $\alpha$  radiation ( $\lambda = 1.54178 \text{ \AA}$ ). The scanning electron microscopy (SEM) images were taken on a JEOL JSM-6700F SEM. The transmission electron microscopy (TEM) was carried out on a JEM-2100F field emission electron microscope at an acceleration voltage of 200 kV. The high-resolution TEM (HRTEM), high-angle annular dark-field scanning transmission electron microscopy (HAADF-STEM) and corresponding elemental mapping analyses were performed on a Thermo Fischer Talos F200X TEM. The nitrogen adsorption-desorption isotherms were obtained by using a Micromeritics ASAP 2460 system, and all the gas adsorption experiments were performed at liquid-nitrogen temperature (77 K). The X-ray photoelectron spectroscopy (XPS) analyses were performed on a VGESCALAB MKII X-ray photoelectron spectrometer with an excitation source of Mg K $\alpha = 1253.6 \text{ eV}$ , and the resolution level was lower than 1 atom%. The ion chromatography (IC) tests were conducted on a Thermo Scientific Dionex Integriion high-pressure IC (HPIC) system.

### **S1.2 Electrocatalytic study**

All the electrochemical measurements were performed in a three-electrode system linked with an electrochemical workstation (CHI660E). All potentials were calibrated to a reversible hydrogen electrode (RHE) and the data were presented without iR correction. An Hg/HgO electrode was used as the reference electrode, a platinum gauze electrode (2 cm  $\times$  2 cm, 60 mesh) was used as the counter electrode, and the as-fabricated catalyst was served as the working electrode which was fixed with an electrode holder connected by a glassy carbon plate. The linear sweeping voltammetry (LSV) tests were conducted at a scan rate of 2 mV s $^{-1}$  in the mixed solution of 1 M KOH and 0.5 M methanol. The electrochemical impedance spectroscopy (EIS) measurements were operated at variable potentials from 10 $^{-2}$ -10 $^5$  Hz at 1.45 V vs. RHE.

## S2. Supplementary Physical and Electrochemical Characterizations

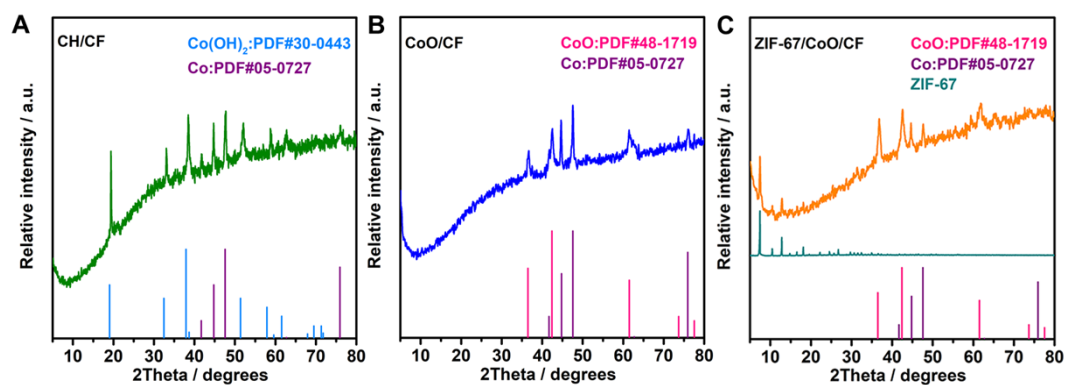


**Fig. S1** XRD patterns of CH/CF (A), CoO/CF (B) and ZIF-67/CoO/CF (C). The reference pattern of ZIF-67 was derived from the powdery sample.

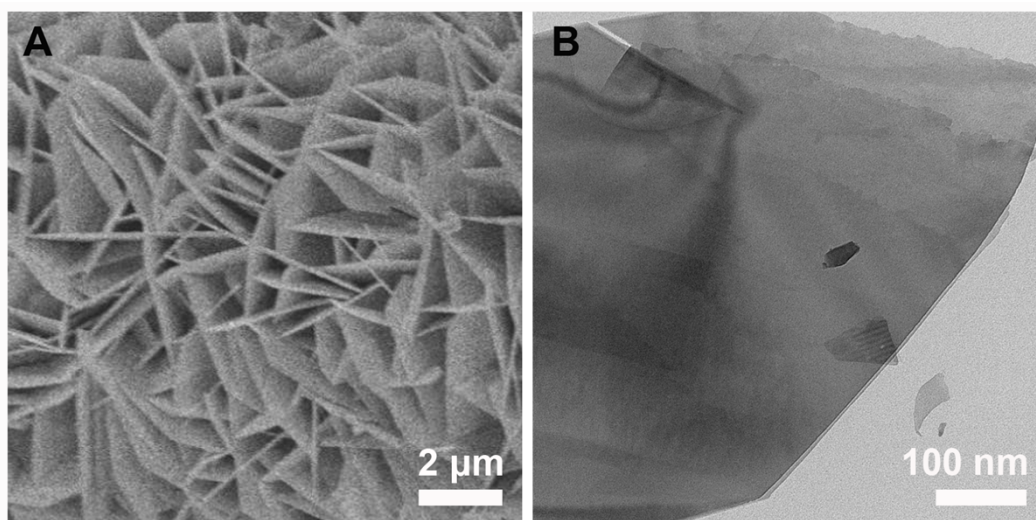


**Fig. S2** (A) SEM and (B) TEM images of CH/CF. Smooth surface of the nanosheets can be clearly identified.

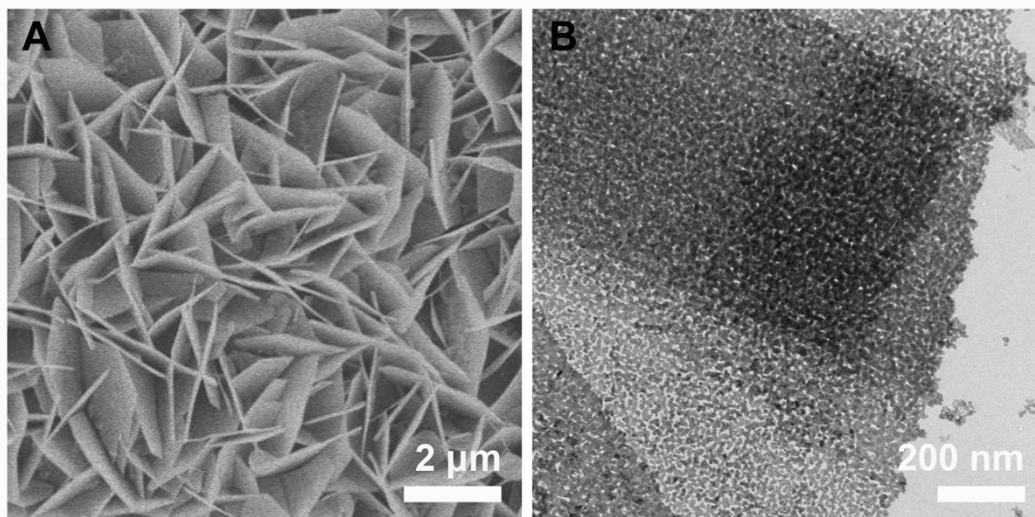


**Fig. S3** (A) SEM and (B) TEM images of CoO/CF. Homogeneous CoO porous nanosheets can be identified owing to the pyrolysis.

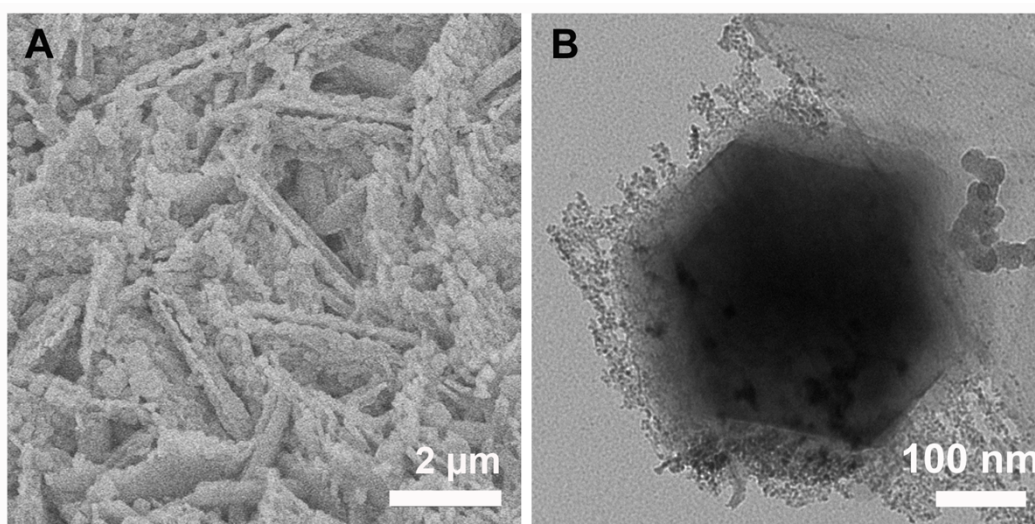


**Fig. S4** (A) SEM and (B) TEM images of ZIF-67/CoO/CF. Benefitted from the high reactivity of the porous surface, ZIF-67 can be generated in both forms of polyhedrons and rough nanosheets, which endows the opportunity for designing N-C conductive highway with highly exposed Co active sites.

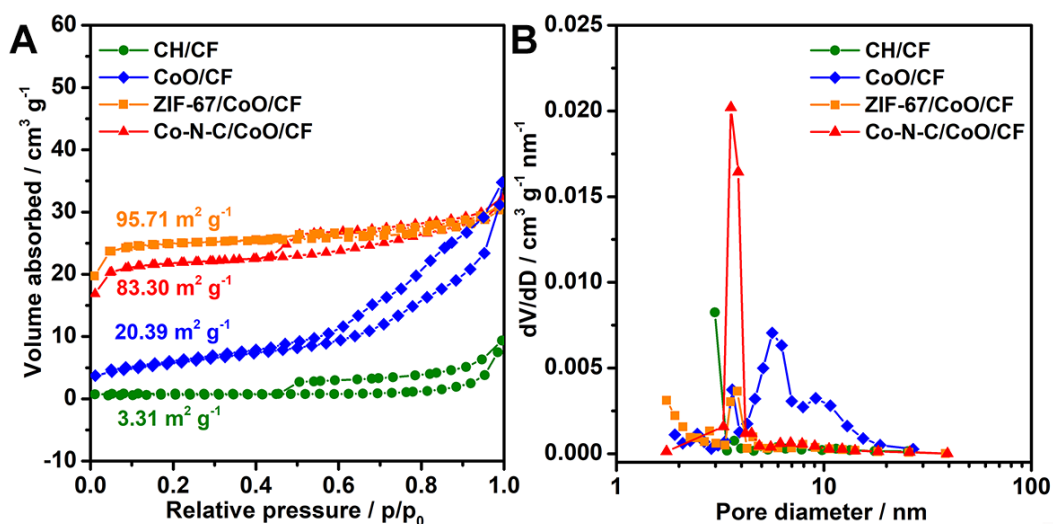


**Fig. S5** (A)  $N_2$  adsorption/desorption isotherm and (B) pore size distribution of the Co-based catalysts.

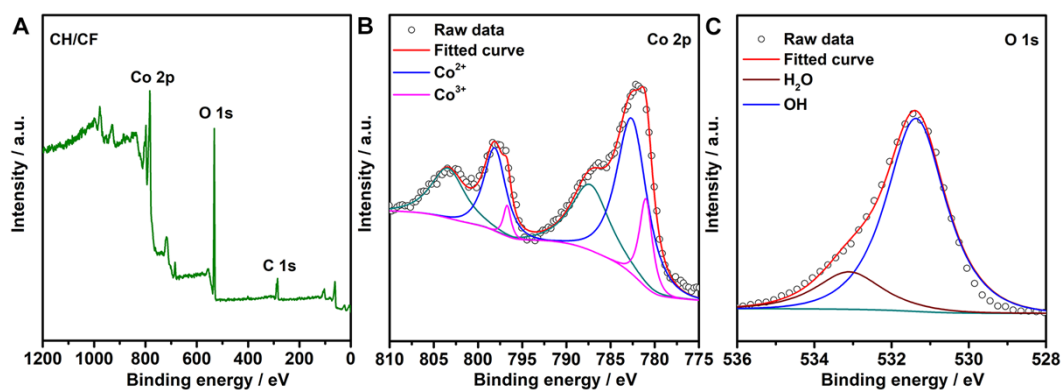


**Fig. S6** XPS spectra of CH/CF for survey data (A), cobalt (B) and oxygen (C).

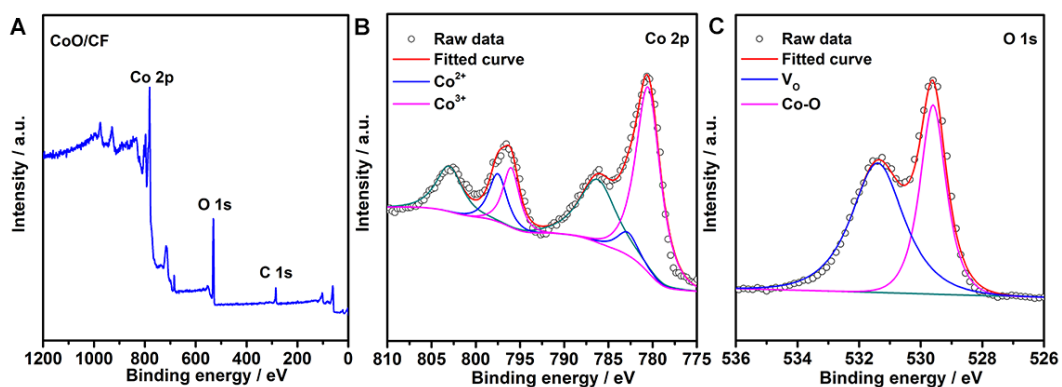


**Fig. S7** XPS spectra of CoO/CF for survey data (A), cobalt (B) and oxygen (C).

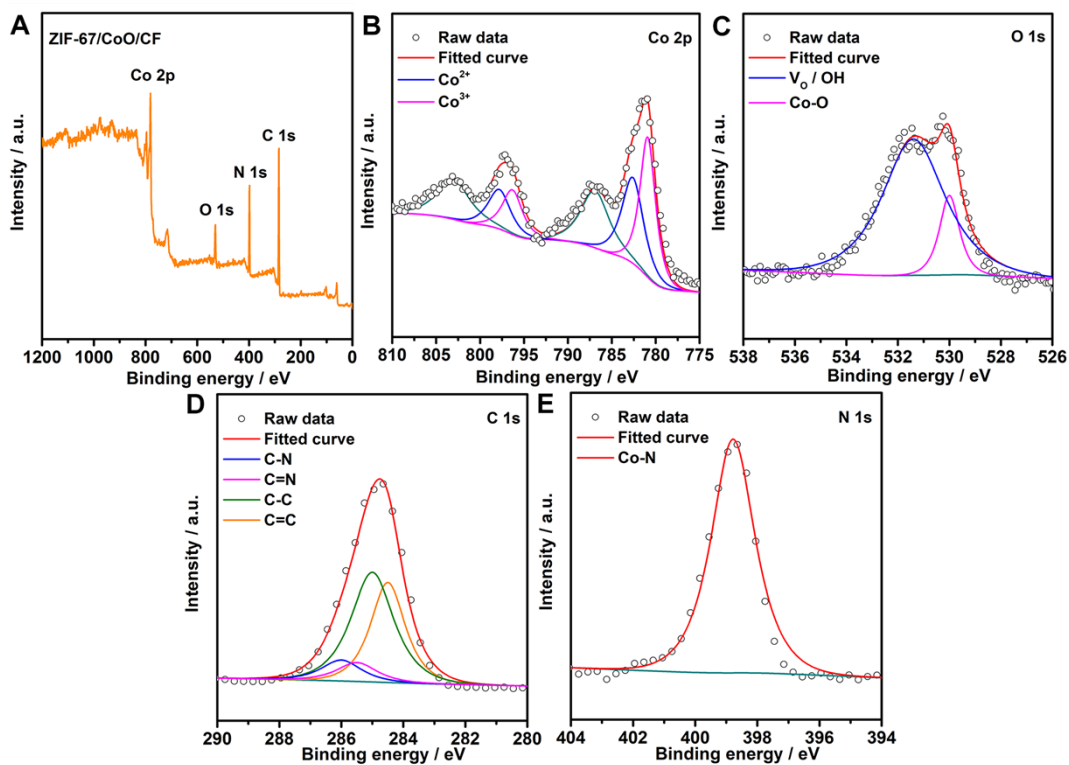


**Fig. S8** XPS spectra of ZIF-67/CoO/CF for survey data (A), cobalt (B), oxygen (C), carbon (D) and nitrogen (E).

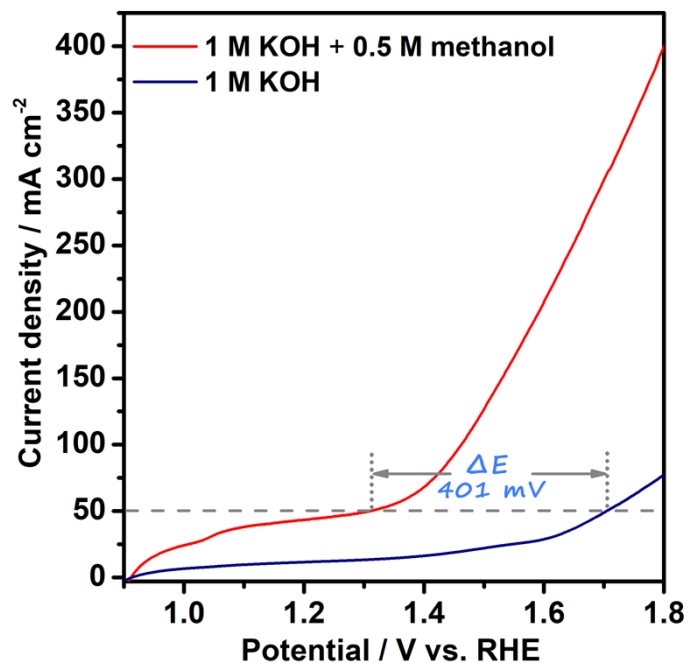


**Fig. S9** The comparison of EMU and OER curves of Co-N-C/CoO/CF. The addition of methanol could lead to a remarkably decreased required potential of 401 mV to reach a 50 mA cm<sup>-2</sup> anodic current density.

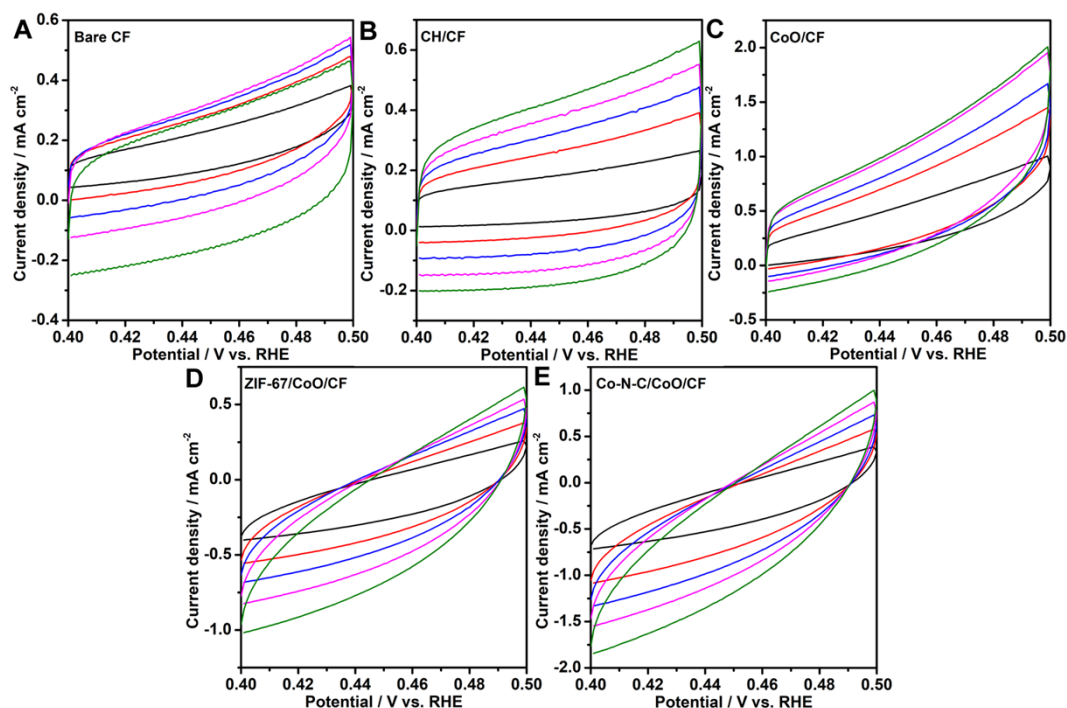


**Fig. S10** Cyclic voltammograms measured in a non-redox region of 0.4~0.5 V vs. RHE. (A) Bare CF, (B) CH/CF, (C) CoO/CF, (D) ZIF-67/CoO/CF and (E) Co-N-C/CoO/CF.

The estimation of the effective active surface area was carried out according to literature.<sup>1, 2</sup> Cyclic voltammetry (CV) tests were conducted at various scan rates (20, 40, 60, 80, 100  $\text{mV s}^{-1}$ ) in the region of 0.4~0.5 V vs. RHE where no redox reaction occurs (Fig. S10), which can be considered as the double-layer capacitive behavior. The electrochemical double-layer capacitance ( $C_{dl}$ ) of the catalysts can be identified from the CV curves, which is expected to be linearly proportional to the electrochemically active surface area. The  $C_{dl}$  value is estimated by plotting the  $\Delta j$  ( $j_a - j_c$ ) at 0.45 V vs. RHE against the scan rates, where the slope is twice  $C_{dl}$ . The  $C_{dl}$  values were listed in Fig. 4C in the main article.

### S3. Product Analysis

The quantitative analysis of the products for electrochemical methanol upgrading was performed by analyzing the data obtained from the ion chromatography (IC) technique. Firstly, we conducted the IC measurements to confirm the retention time of different species. As shown in Fig. S11A, the formate ions ( $\text{HCOO}^-$ ) and hydroxyl ions ( $\text{OH}^-$ ) possess close retention time. Considering the electrolyte in EMU operation is comprised of 1 M KOH and 0.5 M methanol mixed solution, the presence of  $\text{OH}^-$  will inevitably influence the identification and quantification of the as-formed formate ions. In this case, we proposed that purging the alkaline electrolyte with excess  $\text{CO}_2$  could transform the  $\text{OH}^-$  ions into  $\text{HCO}_3^-$  with much longer retention time, thereby providing the opportunity on quantifying the as-generated formate precisely.

In order to precisely quantifying the ionic species in the electrolyte, all the tested electrolytes were diluted by 10 times before conducting the IC measurements. As revealed in Fig. S11B, no signal can be detected for the diluted electrolyte after 3 h EMU operation at 1.4 V vs. RHE apart from the intensive peak contributed by formate and hydroxyl ions, indicating that no ionic contaminant (eg.  $\text{HCO}_3^-$  and  $\text{CO}_3^{2-}$ ) was generated during EMU. We further conducted  $\text{CO}_2$  purging and performed the IC test. As shown in Fig. S11B, the  $\text{CO}_2$  purging could lead to the formation of  $\text{HCO}_3^-$  ions. The signal of  $\text{HCO}_3^-$  ions in the  $\text{CO}_2$ -purging electrolyte is separated from the peak of formate, thus excluding the influence of  $\text{OH}^-$  ions on quantifying formate ions. To quantitative analyze the formate product and evaluate the EMU performance of the catalysts, the calibration curve was plotted by means of IC tests for the formate standard solutions with various concentration (Fig. S11C-D).



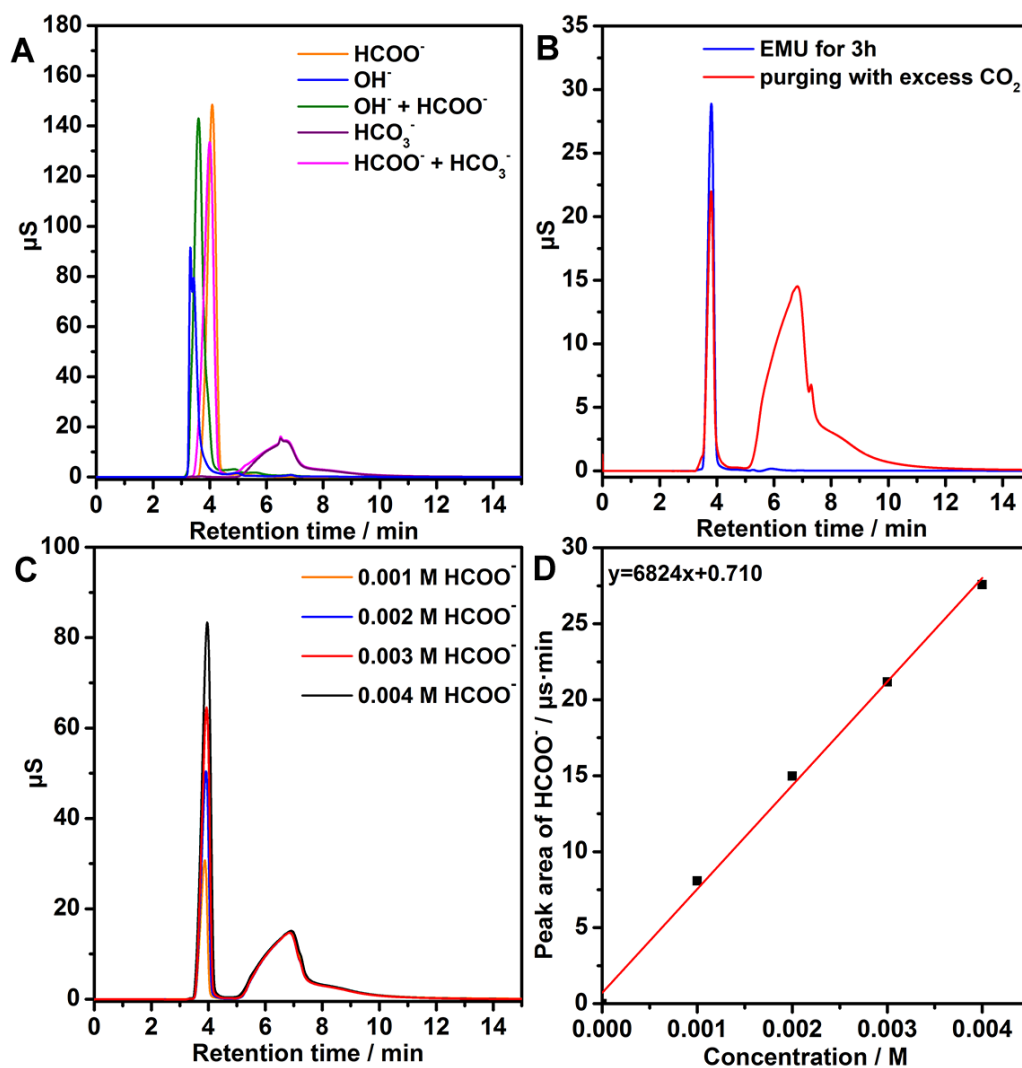


**Fig. S11** (A) IC spectra of  $\text{HCOO}^-$ ,  $\text{OH}^-$ ,  $\text{HCO}_3^-$  and the mixture. (B) Comparison of the IC spectra of the electrolyte after EMU operation for 3 h. Blue line represents the electrolyte without  $\text{CO}_2$  purging, and the red line corresponds to the electrolyte purging with excess  $\text{CO}_2$ . The  $\text{CO}_2$  treatment could eliminate the influence of  $\text{OH}^-$  signal on identifying and quantifying the  $\text{HCOO}^-$  ions and the as-generated  $\text{HCO}_3^-$  shows a completely separated signal to that of  $\text{HCOO}^-$  ions. (C) IC spectra of  $\text{HCOO}^-$  solution with standard concentration. (D) Standard curve of  $\text{HCOO}^-$ .

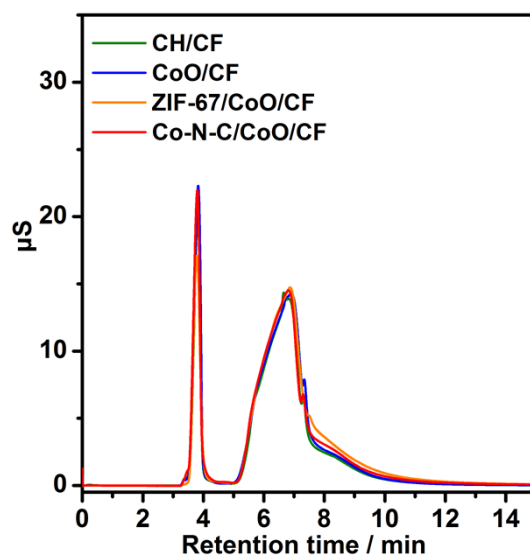


**Fig. S12** IC spectra of Co-N-C/CoO/CF, CoO/CF, ZIF-67/CoO/CF, and CH/CF obtained after 3 h EMU operation at 1.4 V vs. RHE in 25 mL 1 M KOH/0.5 M methanol electrolyte.

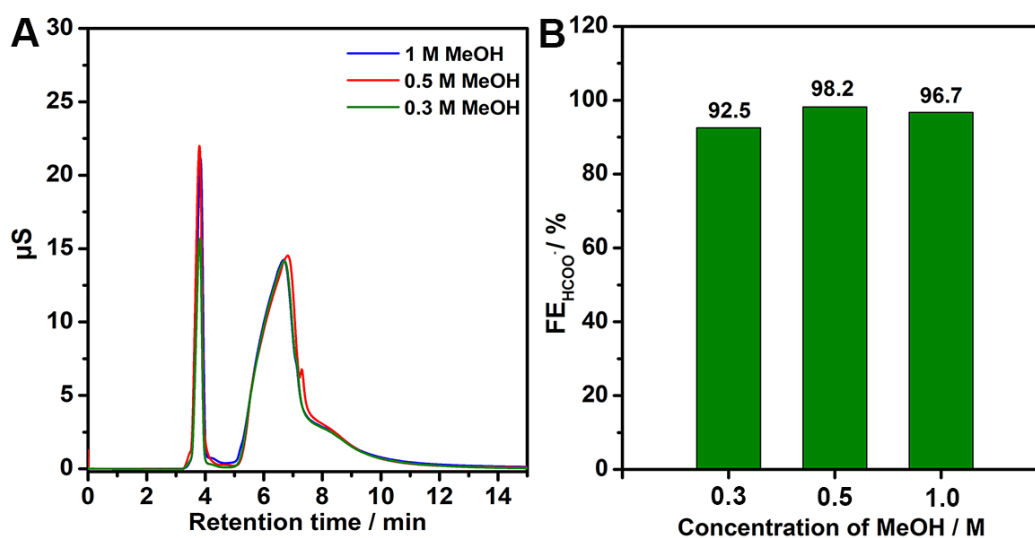


**Fig. S13** (A) Comparison of the IC curves of Co-NC/CoO/CF in 1 M KOH electrolyte with 0.3, 0.5 and 1.0 M methanol after 3 h EMU at 1.4 V vs. RHE. (B) Comparison of the FE of Co-NC/CoO/CF in different concentrations of methanol.

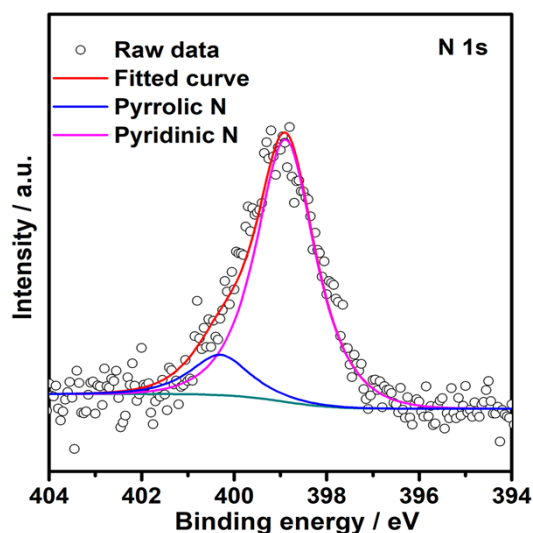


**Fig. S14** Post-catalytic XPS spectrum of nitrogen of Co-N-C/CoO/CF. The pyridinic and pyrrolic nitrogen species can still be revealed after the long-term stability test, which shows negligible difference compared with the pristine XPS N spectrum of Co-N-C/CoO/CF in Fig. 3F, suggesting the high stability of the N-C skeleton during the long-term EMU operation.

## Reference

1. M. A. Lukowski, A. S. Daniel, F. Meng, A. Forticaux, L. Li and S. Jin, *J. Am. Chem. Soc.*, 2013, **135**, 10274-10277.
2. J. Xie, J. Zhang, S. Li, F. Grote, X. Zhang, H. Zhang, R. Wang, Y. Lei, B. Pan and Y. Xie, *J. Am. Chem. Soc.*, 2013, **135**, 17881-17888.